12-2007

Atomic and Electronic Structure of New Hollow-Based Symmetric Families of Silicon Nanoclusters

Pavel V. Avramov
Japan Atomic Energy Agency

Dmitri G. Fedorov
National Institute of Advanced Industrial Science and Technology

Pavel B. Sorokin
L. V. Kirensky Institute of Physics

Leonid A. Chernozatonskii
N. M. Emanuel Institute of Biochemical Physics

Mark S. Gordon
Iowa State University, mgordon@iastate.edu

Atomic and Electronic Structure of New Hollow-Based Symmetric Families of Silicon Nanoclusters

Abstract
We have systematically constructed a set of stable silicon nanocluster families with large arbitrary fullerene-type hollows inside. In addition, conglomerate structures are designed by connecting the nanoclusters through pentagonal and hexagonal junctions. The atomic and electronic structure of the proposed objects is investigated using the semiempirical quantum-mechanical method. It is shown that within each family the band gap and the stability are inversely proportional to the particle effective size. The clusters inherit a wide variety of structural and symmetry properties from their parent silicon fullerenes. The conglomerates confine electrons like quasi-molecules with a peculiar electronic structure related to the junctions. Quantum dots and their conglomerates can host guest atoms in their hollows and therefore present a new promising type of nanomaterials with tunable electronic properties.

Disciplines
Chemistry

Comments
Reprinted (adapted) with permission from *Journal of Physical Chemistry C* 111 (2007): 18824, doi:10.1021/jp0777216.

THE JOURNAL OF PHYSICAL CHEMISTRY C LETTERS

2007, *111,* 18824−18830
Published on Web 12/06/2007

Atomic and Electronic Structure of New Hollow-Based Symmetric Families of Silicon Nanoclusters

Pavel V. Avramov,*,†,‡ Dmitri G. Fedorov,§ Pavel B. Sorokin,‡,||,⊥ Leonid A. Chernozatonskii,|| and Mark S. Gordon#

Takasaki-branch, Advanced Science Research Center, Japan Atomic Energy Agency, Takasaki, 370-1292, Japan, L.V. Kirensky Institute of Physics SB RAS, 660036 Krasnoyarsk, Russian Federation, RICS, National Institute of Advanced Industrial Science and Technology (AIST), 1-1-1 Umezono, Tsukuba, Ibaraki, 305-8568, Japan, N.M. Emanuel Institute of Biochemical Physics of RAS, 119334 Moscow, Russian Federation, Siberian Federal University, 79 Svobodniy av., Krasnoyarsk, 660041 Russia, and Ames National Laboratory/Department of Chemistry, Iowa State University, Ames, Iowa 50011

Received: September 26, 2007; In Final Form: November 10, 2007

We have systematically constructed a set of stable silicon nanocluster families with large arbitrary fullerene-type hollows inside. In addition, conglomerate structures are designed by connecting the nanoclusters through pentagonal and hexagonal junctions. The atomic and electronic structure of the proposed objects is investigated using the semiempirical quantum-mechanical method. It is shown that within each family the band gap and the stability are inversely proportional to the particle effective size. The clusters inherit a wide variety of structural and symmetry properties from their parent silicon fullerenes. The conglomerates confine electrons like quasi-molecules with a peculiar electronic structure related to the junctions. Quantum dots and their conglomerates can host guest atoms in their hollows and therefore present a new promising type of nanomaterials with tunable electronic properties.

I. Introduction

Silicon nanoclusters like nanowires and quantum dots (QDs) have attracted much experimental and theoretical interest recently.[1−8] Porous silicon and silicon nanocrystals (*nc*-Si) precipitated into a SiO_2 matrix are two examples of silicon-based nanoscale systems. Structural investigations show that *nc*-Si particles, having a wide variety of shapes (including quasispherical) and sizes, retain the diamond-like atomic structure of bulk silicon. Although the general crystal lattice type of these species is clear, their exact atomic structure remains unknown.

The *nc*-Si experimental photoluminescence (PL) spectra, obtained for samples synthesized under different conditions (see, e.g., refs 9 and 10) differ from each other very significantly. The PL excitation energies are closely related to the band gap, and the quantum confinement effect (QCE) appears as a band gap dependence on the maximum linear size d of the *nc*-Si particles with $A + Cd^{-k}$ form, where A, C, and k represent the sample-dependent parameters. The pronounced distinctions in QCEs are probably caused by the unresolved differences in the atomic structure of the existing *nc*-Si types.

Several kinds of silicon nanowires and quantum dots have been proposed and studied theoretically. Most species have square or rectangular cross sections, but some nanowires[11] of tetra-, penta-, and hexagonal symmetry as well as quantum dots of tetrahedral,[12] icosahedral, or truncated cubic symmetry[13] have been reported. The icosahedral moiety, having 12 pentagonal vertices and retaining the diamond-like atomic structure, is predicted to have the lowest energy per atom among all small-size nanoparticles ($d \leq 5$ nm). The DFT and semiempirical electronic structure calculations have been applied to study the QCE for structures with different symmetries,[8,14−16] and no deviation from the typical inverse d dependence has been reported.

II. Objects Under Study

The previous theoretical calculations have so far addressed only a limited number of perfect symmetrical types of silicon clusters and have not described all possible shapes of experimental structures. The basic structural tetrahedral units of the silicon lattice have the perfect structure with four <111> facets. The rich diversity of the shapes and sizes of the nanocrystalline silicon can be explained by the chemical binding between *nc*-Si cores at the tetrahedral facets, edges, and vertices. In the simplest case, the combination of 20 tetrahedra results in the formation of the perfect icosahedral silicon nanoclusters.[13] However, there is no reason that other symmetric families of nanoclusters with different numbers of tetrahedra cannot be formed, and we speculate that such objects can partially explain the rich diversity of the *nc*-Si structures.

We now formulate a mathematical definition and a general recipe to generate new silicon nanostructures following the Goldberg polyhedron[17] pattern: nanoclusterss with a desired

* Corresponding author. E-mail: avramov.pavel@jaea.go.jp. Telephone: (81)-27-346-9670. Fax: (81)-27-346-9696.
† Advanced Science Research Center.
‡ L.V. Kirensky Institute of Physics.
§ RICS.
|| N.M. Emanuel Institute of Biochemical Physics.
⊥ Siberian Federal University.
Ames National Laboratory.

10.1021/jp0777216 CCC: $37.00

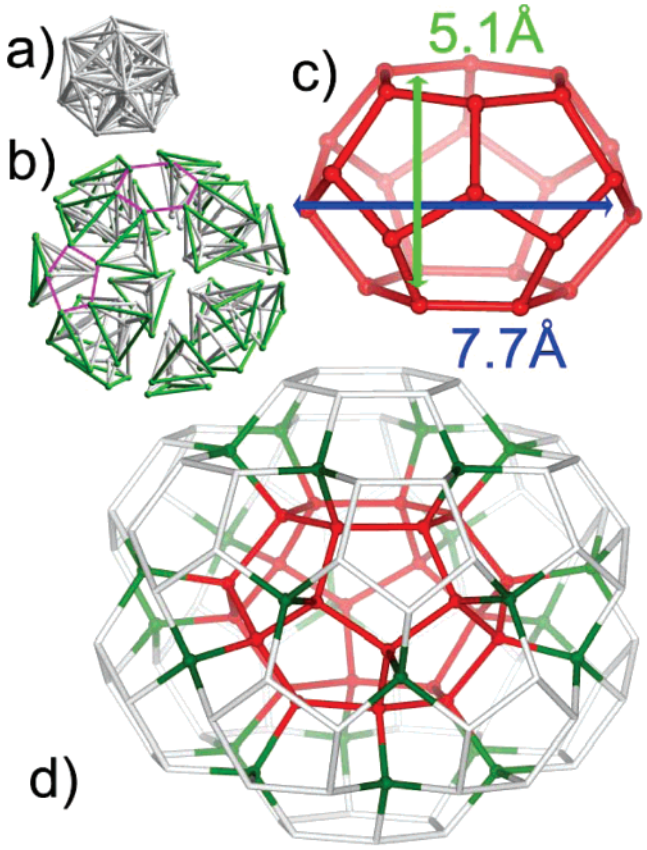

Figure 1. Construction of a typical representative ($2_{24}^{D_{6d}}$) of the new variety of silicon nanoclusters with the inner Si_{24} core of D_{6d} symmetry. (a) 24 silicon tetrahedra Si_5 collapsed into a Goldberg polyhedron. (b) Silicon tetrahedra brought close with a gap between them, forming the $2_{24}^{D_{6d}}$ quantum dot with 24*5 = 120 atoms. The triangular facets of the tetrahedra facing the surface are shown in green. Note that there are no chemical bonds between the vertices of the tetradehra, and their edges are shown for geometrical reasons. Two typical vertices with hexagonal and pentagonal facets involving actual Si−Si bonds are shown in magenta. (c) The Si_{24} hollow inside the quantum dot $2_{24}^{D_{6d}}$ has a low fullerene structure, with the smallest and largest linear dimensions shown. (d) The fully optimized structure of the quantum dot with a hollow (shown in red). The silicon atoms are depicted in layers 1, 2, and 3 in red, green, and gray colors, respectively. Hydrogen atoms terminating unsaturated surface bonds are not shown.

number of pentagonal and hexagonal vertices can be designed by bringing together 20 + n silicon tetrahedra (Figure 1a and b) ($n \geq 4$ is some integer) of the same sizes through three equivalent <111> facets, and the remaining facets (one in each tetrahedron) form the surface of the resultant cluster. The inward vertices of these silicon tetrahedra form low fullerene-like Si_{20+n} regions in the center (Figure 1c), composed of 12 pentagons and n/2 hexagons.

The symmetry of a resulting silicon quantum dot (Figure 1d) is a subgroup of the point group of the parent fullerene, whose pentagons and hexagons are attached by pentagonal/hexagonal channels formed by five/six tetrahedral edges, respectively. The external channel ends are in fact the pentagonal/hexagonal vertices of the nanocluster. The addition of silicon tetrahedra results in some structural tension due to deviations of chemical bonds involving Si from the perfect tetrahedral arrangement (see below). Because of this, only small fullerene-based structures with high-symmetry Si_{24} (D_{6d}), Si_{26} (D_{3h}), and Si_{28} (T_d) (Figure 2) were used in this work as basic units to produce stable QDs; one can, however, use any other symmetry (subgroups of I_h or D_{6d}). The spacious hollow (roughly, 5.1 × 7.7 × 7.7 Å^3) for one quantum dot with the basic Si_{24} fullerene-like core (D_{6d}) is presented in Figure 1c. The hollow is large enough to hold one or several guest ions, atoms, or molecules forming an endohedral complex.

A practical way to design a Goldberg-type quantum dot is the following: on the top of the fullerene core (Figure 1c), a second layer of 20 + n atoms is added. The atoms of the third layer are connected with each other by the atoms forming the surface of the resulting QD with 12 pentagonal and n/2 hexagonal vertices. Using the same procedure, one can add several silicon layers forming a QD of the desired size and symmetry. All quantum dots with L silicon layers built upon the fullerene-like core with m atoms having the point group G can be compactly classified under the notation of L_m^G. For example, the $2_{20}^{I_h}$ and $3_{24}^{D_{6d}}$ symbols denote the two- and three-layered icosahedral ($Si_{100}H_{60}$) and hexagonal ($Si_{336}H_{144}$) structures, respectively.

It is possible to introduce a stoicheometric formula for the species with L silicon layers. The number of silicon atoms in each individual silicon layer l is equal to $m*l^2$, where m is the number of silicon atoms of the core. The number of silicon atoms N_{Si} for a given number of layers L is equal to

$$N_{Si} = m\sum_{l=1}^{L} l^2 = mL(L+1)(2L+1)/6$$

The number of hydrogen atoms saturating the dangling bonds for the silicon layers is given by

$$N_H = m\sum_{l=1}^{L} l = mL(L+1)/2$$

For example, the $3_{24}^{D_{6d}}$ dot has $m = 24$ and $L = 3$; thus, $N_{Si} = 336$ and $N_H = 144$.

To perform a systematic comparative study of the electronic properties of silicon QDs, we also considered a number of structures reported previously, closely related to bulk silicon; cubic (denoted by $C_N^{O_h}$, where the central symbol C is for cubic, the superscript denotes the point group of the basic unit and the subscript shows the number of silicon atoms N in the whole structure), 14-facet truncated cubic ($\dot{C}_N^{O_h}$, where the single dot denotes the truncation of vertices), 26-facet truncated cubic ($\ddot{C}_N^{O_h}$, two dots denote the truncation of the vertices and the edges),[13] octahedral ($O_N^{O_h}$), truncated octahedral ($\dot{O}_N^{O_h}$), and tetrahedral ($T_N^{T_d}$) quantum dots. The tetrahedral and octahedral QDs have four and eight <111> facets, respectively.

Junctions of pentagonal or hexagonal symmetry can be made by cutting off two vertices of a pair of proposed quantum dots and connecting the truncated structures through the resulting cross sections into one conglomerate structure. Let us denote the interfaces through hexagonal and pentagonal vertices by empty (∘) and solid (•) circles, respectively. Such junctions keep the tetrahedral nature of all silicon atoms constituting the structures. We have designed several conglomerates composed of two, three, four, or six QDs of different symmetry, size, and shape (linear, bent, and arranged in a circle c - $(2_{26}^{D_{3h}} \circ 2_{26}^{D_{3h}})_3$ structures, c stands for cyclic, Figure 2). Similar linear structures composed of several icosahedral quantum dots have been obtained in classical MD simulations by freezing the silicon melt in a thin (1.36 nm) nanopore.[18] In multilayered quantum dots ($L \geq 3$), the junctions can be modified by the way the vertices are cut and connected with each other (for details, see Tables 1 and 2).

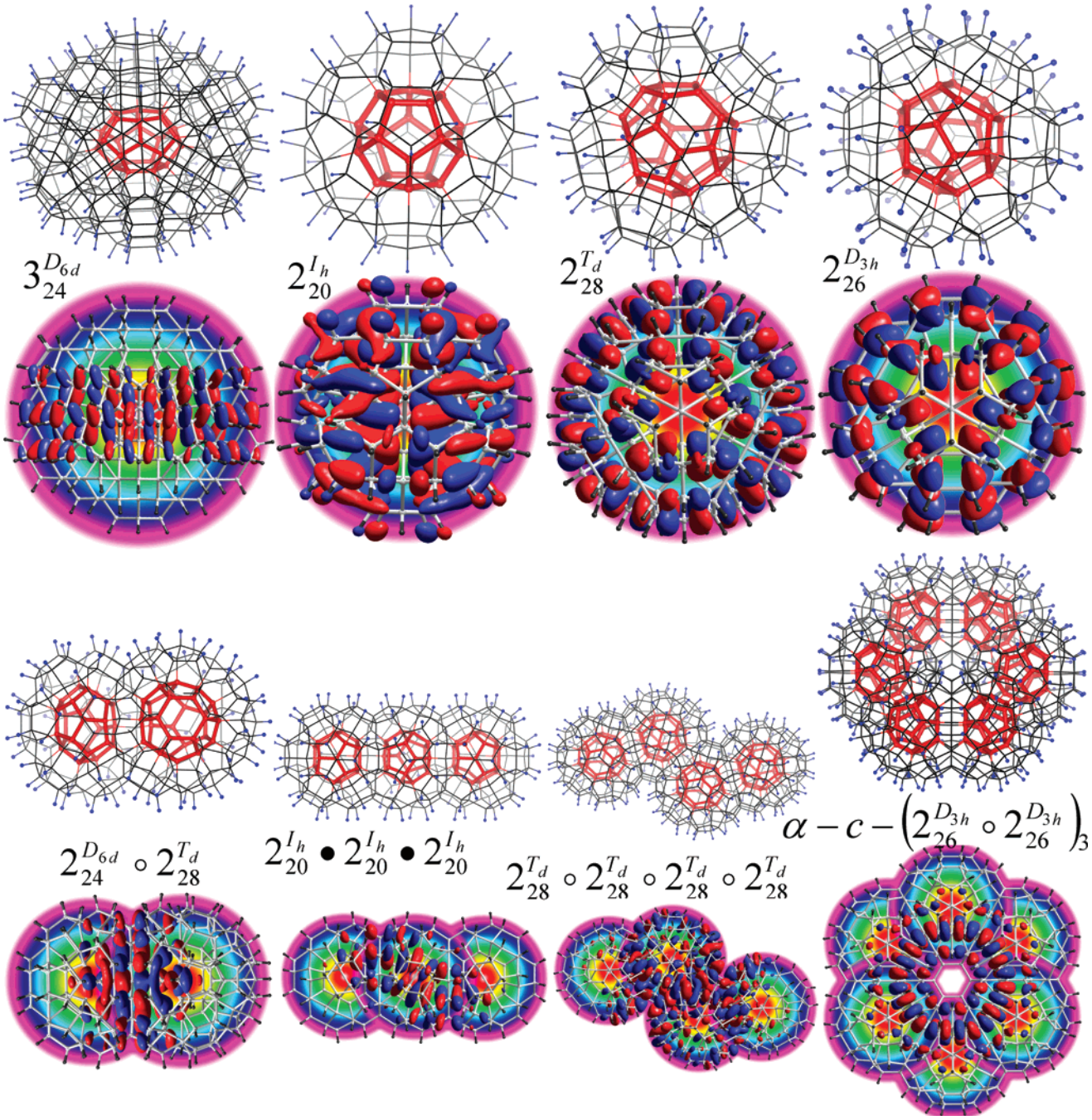

Figure 2. Proposed silicon nanocluster highest occupied molecular orbitals are shown immediately below each structure, for a selected set of the objects (upper part) and their conglomerates (lower part). The two phases of the orbitals are shown in blue and red. The hollows inside the structures are shown in red. The symbols of each structure describe the number of silicon layers, the size, and the symmetry of the central hollow (see main text). Single globe quantum dots (top four objects) are nearly spherical structures and thus atom-like in terms of the electron confinement; the lower four conglomerate quantum dots are multiglobular molecule-like structures. To underline the globular nature of the clusters for some images, we varied the background from purple to red.

III. Method of Electronic Structure Calculations

To study the atomic structure and electronic properties of the proposed silicon nanoclusters, we used the semiempirical Austin Model 1 (AM1)[19] based on the modified neglect of diatomic overlap (MNDO)[20] approximation, which has been successfully employed previously to study the atomic and electronic structures of Si nanoclusters saturated by hydrogen atoms.[8,12,21] AM1 is generally thought to produce very good structures and to systematically overestimate the band gap in silicon clusters. For single quantum dots cut out from bulk silicon, we fitted the band gap to the form of $A + Cd^{-1}$ and obtained its value at the infinite size d, equal to $A = 6.070$ eV. The experimental value in solid crystal silicon is 1.16 eV;[22] thus, we assumed that the AM1 band gap overestimates the experiment by 4.91 eV and this value was subtracted from all AM1 band gap values (Tables 1 and 2). The atomic structure optimization was carried out until the rms gradient became smaller than 0.05 kcal/mol/Å. The point groups were determined based on strict criteria suitable for quantum-mechanical orbital labeling; however, most structures possess a much higher symmetry (Tables 1 and 2) within a minor distortion allowance (in the rms terms, typically about 0.01 Å).

To study the stability, we calculated the energy per silicon atom for all systems. Because of the nearly perfect tetrahedral

TABLE 1: Atomic and Electronic Properties of Single Silicon Nanoclusters (The Energy E_{Si} Per Si Atom Shows Stability)

name	formula	symmetry[a]	min size, nm	max size, nm	HOMO, LUMO	band gap, eV[b]	E_{Si}, kcal/mol	number of unequivalent Si−Si bonds	min/max Si−Si distances, Å
				Trigonal, hexagonal, and tetrahedral (fullerene-derived)					
$2_{26}^{D_{3h}}$	$Si_{130}H_{78}$	C_{3h}/D_{3h}	1.58	1.58	A″,E′	2.028	−1902.11	19	2.334/2.386
$2_{24}^{D_{6d}}$	$Si_{120}H_{72}$	D_{6d}	1.48	1.48	B_1,B_2	1.997	−1902.23	9	2.342/2.382
$2_{28}^{T_d}$	$Si_{140}H_{84}$	C_1/C_{3v}	1.50	1.50	A,A	2.136	−1902.05	10	2.331/2.385
$3_{26}^{D_{3h}}$	$Si_{364}H_{156}$	C_{3h}/D_{3h}	2.35	2.35	A″,E′	1.159	−1910.50	33	2.323/2.421
$3_{24}^{D_{6d}}$	$Si_{336}H_{144}$	D_{6d}	2.24	2.24	B_1,B_2	1.611	−1910.67	22	2.328/2.402
$3_{28}^{T_d}$	$Si_{392}H_{168}$	C_1/S_4	2.33	2.33	A,A	1.686	−1910.40	23	2.328/2.425
				Icosahedral					
$2_{20}^{I_h}$	$Si_{100}H_{60}$	C_i/T_h	1.33	1.33	A_g,A_u	2.284	−1902.74	4	2.321/2.398
$3_{20}^{I_h}$	$Si_{280}H_{120}$	C_i/T_h	2.05	2.05	A_g,A_u	1.847	−1911.26	9	2.304/2.389
$4_{20}^{I_h}$	$Si_{600}H_{200}$	C_1/T_h	2.78	2.78	A,A	1.602	−1916.01	14	2.320/2.389
$5_{20}^{I_h}$	$Si_{1100}H_{300}$	C_1/C_5	3.51	3.51	A,A	1.457	−1918.58	20	2.280/2.387
				Tetrahedral					
$T_{51}^{T_d}$	$Si_{51}H_{52}$	C_1/D_{2d}	0.94	1.15	A,A	2.469	−1883.66		
$T_{87}^{T_d}$	$Si_{87}H_{76}$	C_1/C_{3v}	1.35	1.53	A,A	2.174	−1890.57		
$T_{136}^{T_d}$	$Si_{136}H_{104}$	C_1/S_4	1.64	1.92	A,A	1.972	−1895.75		
$T_{201}^{T_d}$	$Si_{201}H_{138}$	C_1/C_{3v}	1.97	2.30	A,A	1.819	−1899.51		
$T_{281}^{T_d}$	$Si_{281}H_{172}$	C_1/T_d	2.28	2.68	A,A	1.710	−1903.04		
				Octahedral					
$O_{84}^{O_h}$	$Si_{84}H_{64}$	C_1/D_{2d}	1.64	1.64	A,A	2.239	−1895.39		
$O_{286}^{O_h}$	$Si_{286}H_{144}$	C_1/C_3	2.72	2.72	A,A	1.709	−1907.97		
				Truncated octahedral					
$\dot{O}_{80}^{O_h}$	$Si_{80}H_{56}$	D_{2d}	1.35	1.35	E,B_2	2.190	−1897.81		
$\dot{O}_{264}^{O_h}$	$Si_{268}H_{124}$	C_{2v}	2.19	2.19	B_1,B_1	1.697	−1909.63		
				Cubic					
$C_{75}^{O_h}$	$Si_{75}H_{64}$	C_1	1.13	1.35	A,A	2.148	−1890.74		
$C_{88}^{O_h}$	$Si_{88}H_{70}$	C_1	0.96	1.59	A,A	2.118	−1893.68		
$C_{139}^{O_h}$	$Si_{139}H_{92}$	C_1	1.54	1.67	A,A	1.877	−1899.90		
$C_{280}^{O_h}$	$Si_{280}H_{140}$	C_1	1.59	2.43	A,A	1.644	−1907.41		
$C_{368}^{O_h}$	$Si_{368}H_{164}$	C_s	1.88	2.54	A′,A′	1.555	−1909.91		
				Truncated cubic					
$\dot{C}_{123}^{O_h}$	$Si_{123}H_{76}$	C_1	0.96	1.58	A,A	1.890	−1901.68		
$\dot{C}_{323}^{O_h}$	$Si_{323}H_{124}$	C_1/T	1.06	2.28	A,A	1.601	−1912.71		
$\dot{C}_{537}^{O_h}$	$Si_{537}H_{404}$	C_1	2.01	2.74	A,A	1.482	−1913.43		
				Doubly truncated cubic					
$\ddot{C}_{147}^{O_h}$	$Si_{147}H_{76}$	C_1/T_d	1.37	1.66	A,A	1.904	−1906.42		
$\ddot{C}_{287}^{O_h}$	$Si_{287}H_{124}$	C_1/S_4	1.92	2.07	A,A	1.641	−1910.59		
$\ddot{C}_{465}^{O_h}$	$Si_{465}H_{204}$	C_1	2.17	2.65	A,A	1.514	−1910.92		

[a] The structures are often slightly distorted from a higher point group, which is listed after a slash. [b] The AM1 values with the correction of 4.91 eV subtracted.

character of these Si clusters, the energies of hydrogen atoms (E_H) can be assumed to be close to a constant, which we calculated from the difference of the energies of several Si_mH_n and Si_mH_{n-2} tetrahedral clusters to be equal to −356.86 kcal/mol. Consequently, the averaged energy per Si atom in a Si_mH_n structure was defined as $E_{Si} = (E - nE_H)/m$, where E is the semiempirical energy of Si_mH_n. The resulting atomic structures of silicon nanoclusters, described above, can be found in the Supporting Information.[23]

IV. Results and Discussion

The formation of the Goldberg-type nanoclusters affects the perfect tetrahedral structure of silicon. At the AM1 level of theory, the Si−Si distance in the center of the largest silicon tetrahedron $Si_{281}H_{172}$ cluster ($T_{281}^{T_d}$, a good approximation to the bulk silicon) is predicted to be 2.340 Å. Let us consider the typical examples of the proposed clusters (Table 1): The smallest $2_{20}^{I_h}$ structure has four nonequivalent Si−Si bonds with predicted distances of 2.321, 2.332, 2.358, and 2.378 Å; the diameter of the central hollow is 6.536 Å. The deviation from the perfect terahedral values of the bond angles reaches ±2.40°. The central hollow region in $3_{20}^{I_h}$ has a diameter of 6.482 Å and larger deviations of the bond lengths (nine Si−Si bond types, 2.304−2.389 Å) and angles (106.56−111.9°).

The $2_{24}^{D_{6d}}$ structure has larger structural distortions that lead to strain because of the D_{6d} hollow with the smallest and largest dimensions of 5.093 and 7.679 Å, respectively (Figure 1). Both hexagons of the Si_{24} core keep their perfect structure with 120° bond angles and 2.375 Å Si−Si bond lengths. Because of the structural deformation, other angles around the core are smaller (106.22°, 108.08°, and 108.48°) than the perfect tetrahedral value (109.5°). The Si−Si bond lengths (nine types) and angles of other silicon layers vary from 2.342 to 2.375 Å and from 97.58° to 114.52°, respectively (Table 1). Other clusters with different symmetries and sizes demonstrate a large variety of Si−Si bond types, up to 33 in the case of $3_{26}^{D_{3h}}$, for example (Table 1). One can easily study in detail the atomic structure of the proposed

TABLE 2: Properties of the Conglomerate Structures (The Energy E_{Si} Per Si Atom Shows Stability)

name	formula	symmetry[a]	min size, nm	max size, nm	HOMO, LUMO	band gap, eV[b]	E_{Si}, kcal/mol
			$(2^{I_h}_{20})_n$ family				
$2^{I_h}_{20} \bullet 2^{I_h}_{20}$	$Si_{175}H_{90}$	C_5/D_{5h}	1.33	2.14	E_2,A_2	2.018	−1906.85
$2^{I_h}_{20} \bullet 2^{I_h}_{20} \bullet 2^{I_h}_{20}$	$Si_{250}H_{120}$	C_1/D_{5d}	1.33	3.00	A,A	1.931	−1908.49
$2^{I_h}_{20} \bullet 2^{I_h}_{20} \bullet 2^{I_h}_{20} \bullet 2^{I_h}_{20}$	$Si_{325}H_{150}$	C_1/D_{5h}	1.33	3.86	A,A	1.893	−1909.38
			$2^{I_h}_{20} \bullet 3^{I_h}_{20}$ family				
$2^{I_h}_{20} \bullet 3^{I_h}_{20}$	$Si_{355}H_{150}$	C_1/C_{5v}	1.33	2.88	A,A	1.773	−1911.52
$2^{I_h}_{20} \bullet 3^{I_h}_{20} \bullet 2^{I_h}_{20}$	$Si_{430}H_{180}$	C_1/D_5	1.33	3.77	A,A	1.735	−1911.68
			$(3^{I_h}_{20})_n$ family				
α-$3^{I_h}_{20} \bullet 3^{I_h}_{20}$ [c]	$Si_{535}H_{210}$	C_1/D_{5h}	2.05	3.62	A,A	1.652	−1913.03
β-$3^{I_h}_{20} \bullet 3^{I_h}_{20}$ [c]	$Si_{550}H_{210}$	C_s/D_{5h}	2.05	3.60	A″,A″	1.543	−1913.60
γ-$3^{I_h}_{20} \bullet 3^{I_h}_{20}$ [c]	$Si_{490}H_{180}$	C_s/D_{5h}	2.05	3.22	A″,A″	1.655	−1914.18
$3^{I_h}_{20} \bullet 3^{I_h}_{20} \bullet 3^{I_h}_{20}$ [c]	$Si_{700}H_{240}$	C_1/D_{5d}	2.05	4.42	A,A	1.613	−1914.89
			$(2^{D_{6d}}_{24})_n$ family				
$2^{D_{6d}}_{24} \circ 2^{D_{6d}}_{24}$	$Si_{210}H_{108}$	D_{6h}	1.48	2.08	B_{1g},A_{2u}	1.818	−1906.42
$2^{D_{6d}}_{24} \circ 2^{D_{6d}}_{24} \circ 2^{D_{6d}}_{24}$	$Si_{300}H_{144}$	C_1/D_{6d}	1.48	2.94	A,A	1.777	−1908.10
$2^{D_{6d}}_{24} \circ 2^{D_{6d}}_{24} \circ 2^{D_{6d}}_{24} \circ 2^{D_{6d}}_{24}$	$Si_{390}H_{180}$	C_1/D_{6h}	1.48	3.79	A,A	1.752	−1909.00
			$(2^{D_{3h}}_{26})_n$ family				
$2^{D_{3h}}_{26} \circ 2^{D_{3h}}_{26}$	$Si_{230}H_{120}$	C_2/D_{2h}	1.58	2.37	A,B	1.822	−1905.73
$2^{D_{3h}}_{26} \circ 2^{D_{3h}}_{26} \circ 2^{D_{3h}}_{26}$	$Si_{330}H_{162}$	C_1/C_{2v}	1.58	2.96	A,A	1.719	−1907.13
$2^{D_{3h}}_{26} \circ 2^{D_{3h}}_{26} \circ 2^{D_{3h}}_{26} \circ 2^{D_{3h}}_{26}$	$Si_{430}H_{204}$	C_1/C_{2h}	1.58	3.92	A,A	1.669	−1907.88
α-$c - (2^{D_{3h}}_{26} \circ 2^{D_{3h}}_{26})_3$	$Si_{600}H_{252}$	C_2/D_{6h}	1.58	3.23	A,B	1.615	−1910.36
β-$c - (2^{D_{3h}}_{26} \circ 2^{D_{3h}}_{26})_3$	$Si_{564}H_{252}$	C_2/D_{6h}	1.58	3.14	A,B	1.662	−1909.13
			$(2^{T_d}_{28})_n$ family				
$2^{T_d}_{28} \circ 2^{T_d}_{28}$	$Si_{250}H_{132}$	C_i/D_{3d}	1.50	2.60	A_g,A_u	1.980	−1905.48
$2^{T_d}_{28} \circ 2^{T_d}_{28} \circ 2^{T_d}_{28}$	$Si_{360}H_{180}$	C_1/C_{2v}	1.50	3.23	A,A	1.927	−1906.81
$2^{T_d}_{28} \circ 2^{T_d}_{28} \circ 2^{T_d}_{28} \circ 2^{T_d}_{28}$	$Si_{470}H_{228}$	C_1/C_{2h}	1.50	4.16	A,A	1.893	−1907.51
			mixed junction family				
$2^{I_h}_{20} \bullet 2^{D_{6d}}_{24}$	$Si_{195}H_{102}$	C_1/C_s	1.33	2.32	A,A	1.895	−1906.10
$2^{I_h}_{20} \bullet 2^{D_{3h}}_{26}$	$Si_{205}H_{108}$	C_s	1.33	2.38	A″,A′	1.930	−1905.88
$2^{I_h}_{20} \bullet 2^{T_d}_{28}$	$Si_{215}H_{114}$	C_1/C_s	1.33	2.41	A,A	1.959	−1905.63
$2^{D_{6d}}_{24} \circ 2^{D_{3h}}_{26}$	$Si_{220}H_{114}$	C_1/C_{2v}	1.48	2.25	A,A	1.825	−1906.11
$2^{D_{6d}}_{24} \circ 2^{T_d}_{28}$	$Si_{230}H_{120}$	C_1/C_{3v}	1.48	2.36	A,A	1.913	−1905.93
$2^{D_{3h}}_{26} \circ 2^{T_d}_{28}$	$Si_{240}H_{126}$	C_1/C_s	1.58	2.48	A,A	1.894	−1905.64

The structures are often slightly distorted from a higher point group, which is listed after a slash. [b] The AM1 values with the correction of 4.91 eV subtracted. [c] The formation of the linear $2^{I_h}_{20} \bullet 3^{I_h}_{20}$ and $2^{I_h}_{20} \bullet 3^{I_h}_{20} \bullet 2^{I_h}_{20}$ junctions leads to a significant red energy shift (∼0.2 eV) keeping the same incline. Depending on the way to produce the $3^{I_h}_{20} \bullet 3^{I_h}_{20}$ junctions through the outer or inner silicon shells of the $3^{I_h}_{20}$, the resulting band gaps differ up to 0.112 eV. The shortest γ-$3^{I_h}_{20} \bullet 3^{I_h}_{20}$ junction with the interface through the inner silicon layers reveals the largest band gap. The other two types (α and β), having the outer silicon layers with the same length but containing a different number of silicon atoms at the interface, show a decrease of the band gap up to 6.562 and 6.453 eV, respectively. The band gap of the system with a cavity between the two $3^{I_h}_{20}$ parts (α-$3^{I_h}_{20} \bullet 3^{I_h}_{20}$) is similar to that of the shortest γ-$3^{I_h}_{20} \bullet 3^{I_h}_{20}$ system. The similarity of the band gaps for the systems of different length destroys the typical QCE of the linear $3^{I_h}_{20} \bullet 3^{I_h}_{20}$ systems, making it polysemantic.

objects by downloading the corresponding files with coordinates from the Supporting Information.[23]

The conglomerate structures like $L^{I_h}_{20} \bullet L^{I_h}_{20}$ have a slight (∼1%) deviation of the Si−Si bond lengths in the interface region with respect to the parent ($L^{I_h}_{20}$) structures. The symmetric interfaces ($2^{D_{6d}}_{24} \circ 2^{D_{6d}}_{24}$, $2^{D_{3h}}_{26} \circ 2^{D_{3h}}_{26}$, and $2^{T_d}_{28} \circ 2^{T_d}_{28}$) have mirror symmetry interface regions and a similar slight deviation of bond lengths and angles. The asymmetric interfaces, like $2^{D_{6d}}_{24} \circ 2^{D_{3h}}_{26}$, $2^{T_d}_{28} \bullet 2^{D_{3h}}_{26}$, and so forth, have irregular complex atomic structures with unexpected distortions of the interface regions.

The AM1 energetic stability of all systems (Tables 1 and 2) is plotted in Figure 3a. For comparison, the Si atom energy (^{3}P term) at the same level of theory is −1821.81 kcal/mol. Thus, within our definition of the averaged atomic energy in clusters, Si atoms in quantum dots and their conglomerates are predicted to be stabilized by about 80−100 kcal/mol per atom. In the region of 1.2−3.5 nm, the icosahedral quantum dots are the most stable structures, which is in agreement with the earlier density functional theory (DFT) results.[13] The $\ddot{C}^{O_h}_N$ type of structures is second in energy, which was also reported in the DFT study.[13] Some non-monotonic behavior of the $\ddot{C}^{O_h}_N$ and $\dot{C}^{O_h}_N$ curves can be explained by the formation of silicon dimers at the <100> surfaces.[11,16] At the AM1 level of theory in the 1.5−2.24 nm region, the proposed structures of the D_{6d}, D_{3h}, and T_d cores demonstrate higher or closer (like $\dot{C}^{O_h}_N$ and $2^{D_{3h}}_{26}$ clusters, Figure 3a) stabilities than the truncated octahedral structures with energy differences of ∼0.1 kcal/mol per Si atom. Because of the small energy difference, one can expect an existence of all mentioned clusters with the specific size.

The conglomerate stabilities are higher than those of their single parent quantum dots. Excluding the mixed kinds, the stability increases in the inverse proportion to the linear size of the particles. The asymmetrical types of conglomerates (e.g., $2^{I_h}_{20} \bullet 2^{D_{6d}}_{24}$ or $2^{D_{3h}}_{26} \circ 2^{T_d}_{28}$) composed of several nanoclusters of different symmetry have higher stabilities than their building blocks ($2^{I_h}_{20}$ etc.), and they, if made from $2^{I_h}_{20}$, have a lower

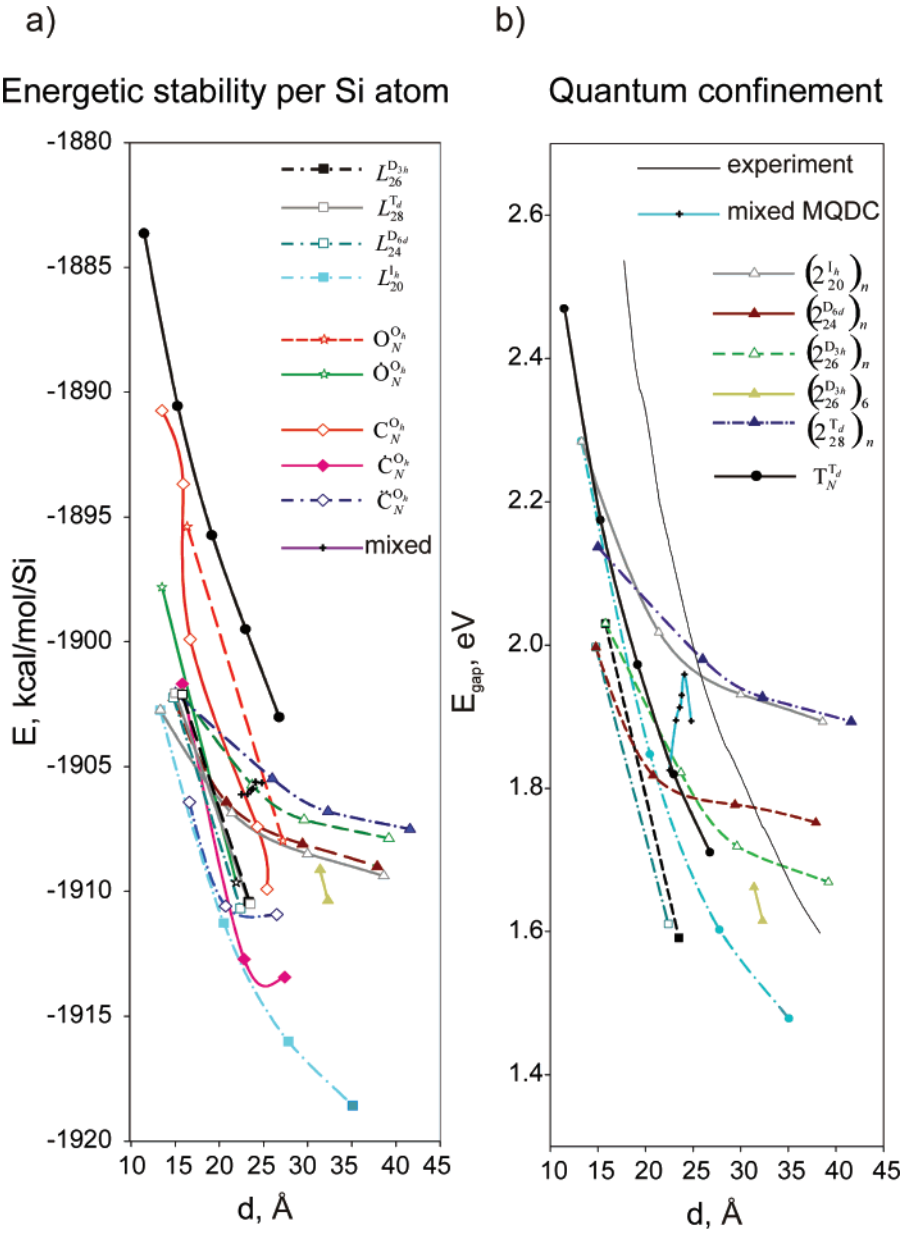

Figure 3. (a) Energetic stability (per Si atom) of the complex silicon nanoclusters vs the effective size d (Å) shown as the following: black dashed line with filled squares ($L_{26}^{D_{3h}}$), as gray line with empty squares ($L_{28}^{T_d}$), dark cyan dashed−dot line with empty squares ($L_{24}^{D_{6d}}$), cyan dashed−dot line with filled squares ($L_{20}^{I_h}$), black line with filled circles ($T_N^{T_d}$), red dashed line with empty five-point star (octahedral, $O_N^{O_h}$), green line with empty five-point star (truncated octahedral, $\dot{O}_N^{O_h}$), brown line with empty diamonds (cubic, $C_N^{O_h}$), pink line with filled diamonds (truncated cubic, $\dot{C}_N^{O_h}$), blue dashed-dot line with empty diamonds (doubly truncated cubic, $\ddot{C}_N^{O_h}$), gray line with empty triangles ($(2_{20}^{I_h})_n$), brown dashed line with filled triangles ($(2_{24}^{D_{6d}})_n$), green dashed line with empty triangles ($(2_{26}^{D_{3h}})_n$ $n = 2$, 3, and 4), gray yellow line with filled triangles (torus, $(2_{26}^{D_{3h}})_6$), blue dashed−dot line with filled triangles ($(2_{28}^{T_d})_n$), and violet line with crosses (asymmetric conglomerates). (b) Band gap (quantum confinement) vs the effective size d (Å), shown as black line (typical experimental[9] QCE of porous silicon), black dashed line with filled squares ($L_{26}^{D_{3h}}$), dark cyan dashed−dot line with empty squares ($L_{24}^{D_{6d}}$), cyan dashed−dot line with filled squares ($L_{20}^{I_h}$), black line with filled circles ($T_N^{T_d}$), gray line with empty triangles ($(2_{20}^{I_h})_n$), brown dashed line with filled triangles ($(2_{24}^{D_{6d}})_n$), green dashed line with empty triangles ($(2_{26}^{D_{3h}})_n$), blue dashed−dot line with filled triangles ($(2_{28}^{T_d})_n$), and gray yellow line with filled triangles (torus, $(2_{26}^{D_{3h}})_6$), cyan solid line with crosses (mixed multiglobular quantum dot conglomerates, MQDC, explained in the text).

stability than the corresponding symmetric conglomerates. The observed increase in the energetic stability with the size is an important point practically in designing and producing nanodevices.

Regardless of the symmetry, the $1/d$ dependence of the band gap upon the linear size is observed within each family (Figure 3b). The QCE curves have different inclines and limiting values and sometimes cross each other, as can be seen for the $2_{24}^{D_{6d}}$- and $2_{26}^{D_{3h}}$-based objects. The presence of junctions in conglomerates changes the QCE; for example, the linear $2_{20}^{I_h} \bullet 2_{20}^{I_h}$ structures reveal a noticeable decrease of the curve slope in comparison with the corresponding single clusters. In general, the conglomerate structures have a somewhat larger band gap than the corresponding single QDs of the same size, caused by the effect of the junction upon the quantum confinement, which can be understood in terms of the quasi-molecular representation of conglomerates; see below. The band-gap dependence of the symmetric conglomerates ($2_{24}^{D_{6d}}$, $2_{26}^{D_{3h}}$, and $2_{28}^{T_d}$) is similar to that of the $2_{20}^{I_h}$-based structures but with smaller values of the band gap energies and curve inclines.

The family of asymmetrical conglomerates ($2_{20}^{I_h} \bullet 2_{24}^{D_{6d}}$, $2_{20}^{I_h} \bullet 2_{28}^{T_d}$, $2_{20}^{I_h} \bullet 2_{26}^{D_{3h}}$, $2_{24}^{D_{6d}} \circ 2_{26}^{D_{3h}}$, $2_{24}^{D_{6d}} \circ 2_{28}^{T_d}$, and $2_{26}^{D_{3h}} \circ 2_{28}^{T_d}$) shows a formal destruction of the typical QCE and a maximum at 2.5 nm. However, this departure from the typical dependence occurs because the set of data corresponds to structures of different types. The same apparent nonsystematic behavior would be seen if one plotted a mixture of simple QDs of different types on a single curve.

Because of the nearly spherical shapes, the excitons in proposed silicon nanoclusters can be described as quasi-atomic states with the symmetry labeling in the atomic group K_h.[24] The multiglobular objects introduced in this work can be thought of as quasi-molecular objects (Figure 2). The structures consisting of two globules (e.g., $2_{20}^{I_h} \bullet 2_{20}^{I_h}$) are quasi-diatomics, for which excitons can be labeled in $D_{\infty h}$. Some quasi-molecular conglomerates retain the full symmetry, even with the detailed atomic structure taken into consideration (e.g., the bent structure of $2_{28}^{T_d} \circ 2_{28}^{T_d} \circ 2_{28}^{T_d} \circ 2_{28}^{T_d}$ in C_{2h} symmetry), whereas linear structures like $2_{20}^{I_h} \bullet 2_{20}^{I_h} \bullet 2_{20}^{I_h} \bullet 2_{20}^{I_h}$ and $2_{24}^{D_{6d}} \circ 2_{24}^{D_{6d}} \circ 2_{24}^{D_{6d}} \circ 2_{24}^{D_{6d}}$ with D_{5h} and D_{6h} symmetry, respectively, are not much below the full group of $D_{\infty h}$.

The highest occupied molecular orbitals (HOMO), Figure 2, describe the Si−Si σ bonds delocalized over many pairs of atoms. The sign alternation between neighbors is commonly seen in all structures (see the intermingled blue and red orbital droplets for $3_{24}^{D_{6d}}$), with some orbital clouds assembled in larger nebular aggregates between the silicon layers, as can be seen for $2_{20}^{I_h}$. The HOMO localization in conglomerates is quite interesting: although for the symmetric ("$D_{\infty h}$") type much density remains inside the globules ($2_{20}^{I_h} \bullet 2_{20}^{I_h} \bullet 2_{20}^{I_h}$ and α-c − $(2_{26}^{D_{3h}} \circ 2_{26}^{D_{3h}})_3$) and pronounced nodes between globules are often found, for the asymmetric kind ("$C_{\infty v}$") HOMOs are strongly localized in the interglobule junction area (e.g., $2_{24}^{D_{6d}} \circ 2_{28}^{T_d}$). The reason for this behavior is the increased tension between globules, which is expressed in the higher orbital energies, pushing one junction MO to become the HOMO localized in the interglobule junction area ($2_{28}^{T_d} \circ 2_{28}^{T_d} \circ 2_{28}^{T_d} \circ 2_{28}^{T_d}$) or on the inner ring for the torus c - $(2_{26}^{D_{3h}} \circ 2_{26}^{D_{3h}})_3$. To underline the globular nature of the clusters for images with depicted orbitals, we varied the background from purple to red.

The view of the multiglobular structures as quasi-polyatomics can be developed further by considering the orbitals in the junction area to be orbitals describing the chemical bonding between quasi-atoms (globules). The HOMO for $2_{24}^{D_{6d}} \circ 2_{28}^{T_d}$ shows the opposite phases between the globules, and thus one can speculate that this HOMO actually looks like the occupied antibonding orbital between quasi-atoms, whereas for $2_{28}^{T_d} \circ 2_{28}^{T_d} \circ 2_{28}^{T_d} \circ 2_{28}^{T_d}$ some shared electron density between globules can be seen, purporting a certain bonding character.

V. Conclusions

In this work, based on the fullerene-like central silicon cores, we proposed and systematically classified new families of silicon nanoclusters of adjustable symmetry. The central hollows can accommodate one or more guest atoms or molecules, and the interplay of several hosts in conglomerates can lead to promising novel types of nanodevices. All structures are stable minima on the energy surface and display an increased stability and decreased band gap with the linear size. The detailed structural information can be used to aid the analysis of the experimental data; for example, if mass or Raman spectra are measured, then the structures can be matched with the symmetries and chemical formulas we have provided here.

The low silicon fullerene cores determine the symmetric properties of the hollows in the nanoclusters and their conglomerates; this is especially important for the endohedral complexes when the symmetry of the hollow directly controls the electronic structure splitting of the guest. The combination of all predicted structural, symmetric, and electronic properties of the proposed objects has the potential to open a new field of applications in nanoscience and nanotechnology.

Acknowledgment. This work was partially supported by the project "Material Design with New Functions Employing Energetic Beams" and JAEA Research fellowship (P.V.A.), by Russian Fund of Basic Researches (grant no. 05-02-17443), grants from the U.S. Department of Energy via the Ames Laboratory and the Air Force Office of Scientific Research, grant of Deutsche Forschungsgemeinschaft and Russian Academy of Sciences, no. 436 RUS 113/785 (LAC). P.V.A. also acknowledges the members of "Research Group for Atomic-scale Control for Novel Materials under Extreme Conditions" Prof. H. Naramoto, Prof. Y. Maeda, Dr. K. Narumi, and Dr. S. Sakai for fruitful discussions and hospitality and Prof. Boris Yakobson for the initial question.

Supporting Information Available: The atomic coordinates of all proposed silicon nanostructures. This material is available free of charge via the Internet at http://pubs.acs.org.

References and Notes

(1) Xu, X.; Sun, B.; Berman, P. R.; Steel, D. G.; Bracker, A. S.; Gammon, D.; Sham, L. J. *Science* **2007**, *317*, 929.
(2) Wang, Y.; Schmidt, V.; Senz, S.; Gösele, U. *Nat. Nanotechnol.* **2006**, *1*, 186.
(3) McAlpine, M. C.; Ahmad, H.; Wang, D.; Heath, J. R. *Nat. Mater.* **2007**, *6*, 379.
(4) Goswami, S.; Slinker, K. A.; Friesen, M.; McGuire, L. M.; Truitt, J. L.; Tahan, C.; Klein, L. J.; Chu, J. O.; Mooney, P. M.; van der Weide, D. W.; Joynt, R.; Coppersmith, S. N.; Eriksson, M. A. *Nat. Phys.* **2007**, *3*, 41.
(5) Avramov, P. V.; Chernozatonskii, L. A.; Sorokin, P. B.; Gordon, M. S. *Nano Lett.* **2007**, *7*, 2063.
(6) Nishiguchi, K.; Zhao, X.; Oda, S. *J. Appl. Phys.* **2002**, *92*, 2748.
(7) Cullis, A. G.; Canham, L. T. *Nature* **1991**, *353*, 335.
(8) Cullis, A. G.; Canham, L. T.; Calcott, P. D. J. *J. Appl. Phys.* **1997**, *82*, 909.
(9) Wolkin, M. V.; Jorne, J.; Fauchet, P. M.; Allan, G.; Delerue, C. *Phys. Rev. Lett.* **1999**, *82*, 197.
(10) Wilcoxon, J. P.; Samara, G. A.; Provencio, P. N. *Phys. Rev. B* **1999**, *60*, 2704.
(11) Zhao, Y.; Yakobson, B. *Phys. Rev. Lett.* **2003**, *91*, 035501.
(12) Filonov, A. B.; Ossicini, S.; Bassani, F.; d'Avitaya, F. A. *Phys. Rev. B* **2002**, *65*, 195317.
(13) Zhao, Y.; Kim, Y.-H.; Du, M.-H.; Zhang, S. B. *Phys. Rev. Lett.* **2004**, *93*, 015502.
(14) Caldas, M. J. *Phys. Status Solidi B* **2000**, *217*, 641.
(15) Garoufalis, C. S.; Zdetsis, A. D.; Grimme, S. *Phys. Rev. Lett.* **2001**, *87*, 276402.
(16) Avramov, P. V.; Kuzubov, A. A.; Fedorov, A. S.; Sorokin, P. B.; Tomilin, F. N.; Maeda, Y. *Phys. Rev. B* **2007**, *75*, 205427.
(17) Goldberg, M. *Tohoku Math. J.* **1937**, *43*, 104.
(18) Nishio, K.; Morishita, T.; Shinoda, W.; Mikami, M. *J. Chem. Phys.* **2006**, *125*, 074712.
(19) Dewar, M. J. S.; Zoebisch, E. G.; Healy, E. F.; Stewart, J. J. P. *J. Am. Chem. Soc.* **1985**, *107*, 3902.
(20) Stewart, J. J. P. *J. Comput. Chem.* **1989**, *10*, 209.
(21) Mazzone, A. M. *Phys. Rev. B* **1996**, *54*, 5970.
(22) Sze, S. M. *The Physics of Semiconductor Devices*; Wiley: New York, 1969.
(23) http://staff.aist.go.jp/d.g.fedorov/Struct-nc-Si.zip.
(24) Scholes, G. D.; Rumbles, G. *Nat. Mater.* **2006**, *5*, 683.